Transverse-Mass Spectra in Heavy-Ion Collisions at energies $E_{\text{lab}} = 2$–160 GeV/nucleon

Yu.B. Ivanov[1, 2, *] and V.N. Russkikh[1, 2, †]

^{1}*Gesellschaft für Schwerionenforschung mbH, Planckstr. 1, D-64291 Darmstadt, Germany*
^{2}*Kurchatov Institute, Kurchatov sq. 1, Moscow 123182, Russia*

Transverse-mass spectra of protons, pions and kaons produced in collisions of heavy nuclei are analyzed within the model of 3-fluid dynamics. It was demonstrated that this model consistently reproduces these spectra in wide ranges of incident energies, $4A$ GeV $\lesssim E_{\text{lab}} \lesssim 160A$ GeV, rapidity bins and centralities of the collisions. In particular, the model describes the "step-like" dependence of kaon inverse slopes on the incident energy. The key point of this explanation is interplay of hydrodynamic expansion of the system with its dynamical freeze-out.

I. INTRODUCTION

One of the major goals of high-energy heavy-ion research is to explore properties of strongly interacting matter, particularly its phase structure [1]. A great body of experimental data has been already accumulated by now. Theoretical analysis of these data is still in progress. Explanation of transverse-mass spectra of hadrons (especially kaons) in collisions of heavy nuclei turned out to be one of the most difficult tasks [2, 3, 4].

Experimental data on transverse-mass spectra of kaons produced in central Au+Au [5] and Pb+Pb [6, 7] collisions reveal peculiar dependence on the incident energy. The inverse-slope parameter (so called effective temperature T) of these spectra at midrapidity increases with incident energy in the energy domain of BNL Alternating Gradient Synchrotron (AGS) and then saturates at energies of CERN Super Proton Synchrotron (SPS). In Refs. [8, 9] it was assumed that this saturation is associated with the deconfinement phase transition. This assumption was indirectly confirmed by the fact that microscopic transport models, based on hadronic degrees of freedom, failed to reproduce the observed behavior of the kaon inverse slope [2, 3]. Hydrodynamic simulations of Ref. [4] succeeded to describe this behavior. However, in order to reproduce it these hydrodynamic simulations required incident-energy dependence of the freeze-out temperature which almost repeated the shape of the corresponding kaon effective temperature. This happened even in spite of using an equation of state (EoS) involving a phase transition into the quark-gluon plasma (QGP). This way, the puzzle of kaon effective temperatures was just translated into a puzzle of freeze-out temperatures. Moreover, results of Ref. [4] imply that peculiar incident-energy dependence of the kaon effective temperature may be associated with dynamics of freeze-out.

In Ref. [10] it was shown that dynamical description of freeze-out [11], accepted in the model of 3-fluid dynamics (3FD) [12, 13, 14, 15], naturally explains the incident energy behavior of inverse-slope parameters of transverse-mass spectra observed in experiment. This freeze-out dynamics, effectively resulting in a pattern similar to that of the dynamic liquid–gas transition, differs from conventionally used freeze-out schemes. In the brief letter [10] only midrapidity inverse-slope parameters in central collisions were presented. In the present paper we would like to extend analysis of Ref. [10] by presenting transverse-mass spectra themselves at various impact parameters and rapidities and compare them with available experimental data in the range from AGS to SPS incident energies. These spectra are computed with the same set of model parameters as that summarized in Ref. [12]. In particular, the hadronic EoS [16] with incompressibility $K = 210$ MeV is used.

II. THE 3FD MODEL

The 3FD model is designed for simulating heavy-ion collisions in the range from AGS to SPS energies. Unlike the conventional hydrodynamics, where local instantaneous stopping of projectile and target matter is assumed, a specific feature of the dynamic 3-fluid description is a finite stopping power resulting in a counter-streaming regime of leading baryon-rich matter. This counter-streaming is described in terms of two interacting baryon-rich fluids, initially associated with constituent nucleons of the projectile (p) and target (t) nuclei. In addition, newly produced particles, populating the midrapidity region, are associated with a baryon-free "fireball" (f) fluid.

We have started our simulations [10, 12, 14] with a simple hadronic EoS [16]. The 3FD model turned out to be able to reasonably reproduce a large body of experimental data [10, 12, 14] in a wide energy range from AGS to SPS. This was done with a unique set of model parameters summarized in Ref. [12]. Problems were met in

*e-mail: Y.Ivanov@gsi.de
†e-mail: russ@ru.net

description of the transverse flow [14]. The directed flow required a softer EoS at top AGS and SPS energies (in particular, this desired softening may signal occurrence of the phase transition into the QGP).

The transverse-mass spectra are most sensitive to the freeze-out parameters of the model. In the 3FD model the same freeze-out procedure is applied to both the thermal and chemical processes. Normalization of the meson spectra is directly related to the freeze-out temperature. Inverse slopes of the transverse-mass spectra represent a combined effect of the temperature and collective transverse flow of the hydrodynamical expansion. Had it been only the effect of thermal excitation, inverse slopes for different hadronic species would approximately equal. The collective transverse flow makes them different. These two effects partially compensate each other: the later freeze-out occurs, the lower temperature and the stronger collective flow are. Nevertheless, inverse slopes turn out to be sensitive to the instant of the freeze-out. Below we demonstrate that not only slopes but also normalizations of the pion transverse-mass spectra are well described by this unified chemical-thermal freeze-out. Situation with kaons is more delicate, since we have to take into account the associative production of strangeness giving rise to a strangeness suppression factor.

Freeze-out procedure adopted in the 3FD model was analyzed in detail in Ref. [11]. This method of freeze-out can be called dynamical, since the freeze-out process here is integrated into fluid dynamics through hydrodynamic equations. The freeze-out front is not defined just "geometrically" on the condition of the freeze-out criterion met[1] but rather is a subject the fluid evolution. It competes with the fluid flow and not always reaches the place where the freeze-out criterion is met. This kind of freeze-out is similar to the model of "continuous emission" proposed in Ref. [17]. There the particle emission occurs from a surface layer of the mean-free-path width. In our case the physical pattern is similar, only the mean free path is shrunk to zero. We would like to mention that recently the continuous emission model was further microscopically developed [18, 19].

In particular, this dynamical freeze-out results in a peculiar incident-energy dependence of the actual freeze-out energy density averaged over space–time evolution of the collision, $\langle\varepsilon_{\text{out}}\rangle$, see Fig. 1. As seen, $\langle\varepsilon_{\text{out}}\rangle$ reveals fast rise at AGS energies and saturation at the SPS energies. This happens in spite of the fact that our freeze-out condition involves only a single constant parameter—the "triger" freeze-out energy density $\varepsilon_{\text{frz}} = 0.4$ GeV/fm³— which was taken the same for all incident energies with the exception of low incident energies, for which we used lower values: $\varepsilon_{\text{frz}}(2A \text{ GeV}) = 0.3$ GeV/fm³ and
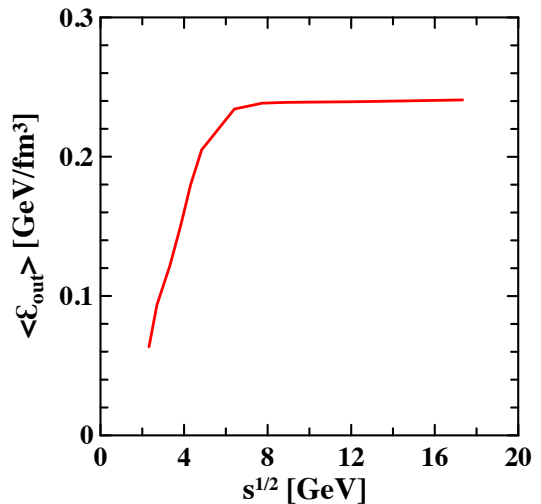

FIG. 1: (Color online) Actual average freeze-out energy density in central Pb+Pb collisions as a function of invariant incident energy.

$\varepsilon_{\text{frz}}(1A \text{ GeV}) = 0.2$ GeV/fm³. In our previous paper [12] we have performed only a rough analysis of this kind[2]. To find out the actual value of ε_{out}, we analyzed results of actual simulations [11].

The "step-like" behavior of $\langle\varepsilon_{\text{out}}\rangle$ is a consequence of the freeze-out dynamics, as it was demonstrated in Ref. [11]. At low (AGS) incident energies, the energy density achieved at the border with vacuum, ε^s, is lower than ε_{frz}. Therefore, the surface freeze-out starts at lower energy densities. It further proceeds at lower densities up to the global freeze-out because the freeze-out front moves not faster than with the speed of sound, like any perturbation in the hydrodynamics. Hence it cannot overcome the supersonic barrier and reach dense regions inside the expanding system. With the incident energy rise the energy density achieved at the border with vacuum gradually reaches the value of ε_{frz} and then even overshoot it. If the overshoot happens, the system first expands without freeze-out. The freeze-out starts only when ε^s drops to the value of ε_{frz}. Then the surface freeze-out occurs really at the value $\varepsilon^s \approx \varepsilon_{\text{frz}}$ and thus the actual freeze-out energy density saturates at the value $\langle\varepsilon_{\text{out}}\rangle \approx \varepsilon_{\text{frz}}/2$, i.e. at the half fall from ε^s to zero. This freeze-out dynamics is quite stable with respect to numerics [11].

Fig. 2 clarifies this "step-like" behavior in terms of the average temperature, transverse velocity and baryon density achieved at the freeze-out in central Au+Au (at AGS energies, impact parameter $b = 2$ fm) and Pb+Pb (at

---

[1] The freeze-out criterion demands that the energy density of the matter is lower than some value ε_{frz}.

[2] This is why in the main text of Ref. [12] we mentioned the value of approximately 0.2 GeV/fm³ for ε_{out} and in the appendix explained how the freeze-out actually proceeded. In terms of Ref. [12] ($\varepsilon_{\text{frz}[1]}$ and $\varepsilon_{\text{frz}[1]}^{\text{code}}$) our present quantities are $\varepsilon_{\text{frz}} = \varepsilon_{\text{frz}[1]}^{\text{code}}$ and $\varepsilon_{\text{out}} = \varepsilon_{\text{frz}[1]}$.
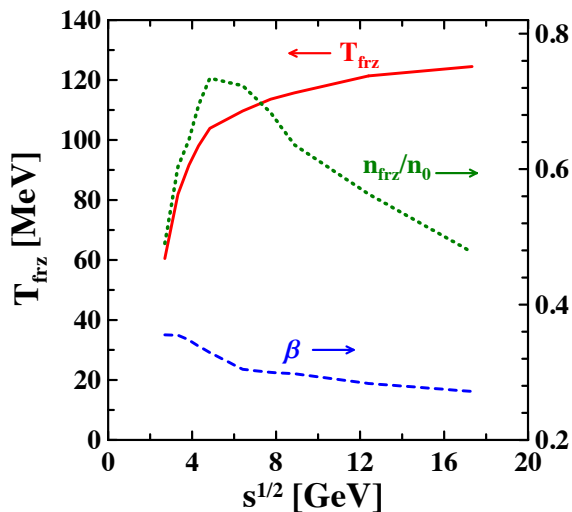
FIG. 2: (Color online) Average temperature (T_{frz}, see scale at the l.h.s. axis), transverse velocity ($\beta = v_T/c$, see scale at the r.h.s. axis) and baryon density over the normal nuclear density (n_{frz}/n_0, see scale at the r.h.s. axis) at the freeze-out in central Au+Au (at AGS energies) and Pb+Pb (at SPS energies) collisions as a function of invariant incident energy. Arrows point to the proper axis scale.
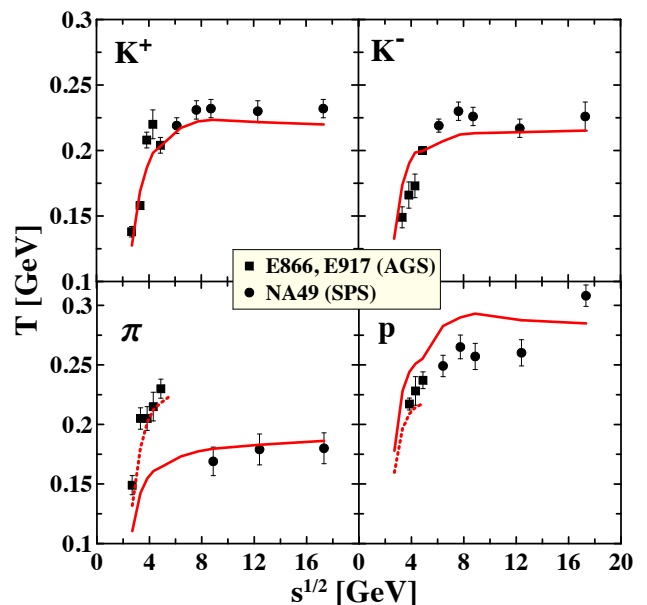

FIG. 3: (Color online) Inverse-slope parameters of transverse-mass spectra of kaons, pions and protons at midrapidity produced in central Au+Au and Pb+Pb collisions as a function of invariant incident energy. Solid lines correspond to purely exponential fit by Eq. (1) with $\lambda = 0$, while dashed lines, as well as experimental data at AGS energies, correspond to fits with $\lambda = -1$ for pions and with $\lambda = 1$ for protons. Experimental data are from Refs. [5, 6, 7, 23, 24].

SPS energies, $b = 2.5$ fm) collisions. The freeze-out temperature T_{frz} reveals a similar "step-like" behavior. At SPS energies the freeze-out temperatures in Fig. 2 are noticeably lower than those deduced from hadron multiplicities in the statistical model [20, 21]. The reason for this is as follows. Whereas the statistical model assumes a single uniform fireball, in the 3FD simulations at the late stage of the evolution the system effectively consists of several "fireballs": two overlapping fireballs (one baryon-rich and one baryon-free) at lower SPS energies and three fireballs (two baryon-rich and one baryon-free) at top SPS energies [11]. At the top SPS energies these three fireballs turn out to be even spatially separated. Therefore, whereas high multiplicities of mesons and antibaryons are achieved by means of high temperatures in the statistical model, the 3FD model explains them by an additional contribution of the baryon-free fireball at a lower temperature. The freeze-out baryon density n_{frz} exhibits a maximum at incident energies of $E_{lab} = 10A$–$30A$ GeV which are well within range of the planned FAIR in GSI. This observation agrees with that deduced from the statistical model [22], even baryon density values in the maximum are similar to those presented in Ref. [22].

This dynamics of the freeze-out is of key importance for explanation of the transverse-mass spectra. In particular, the "step-like" behavior of inverse slopes (effective temperatures) in Fig. 3 is related to the similar "step-like" behavior of $\langle \varepsilon_{out} \rangle$ (see Fig. 1) or freeze-out temperature T_{frz} (Fig. 2). Of course, this relation is not direct, since the collective transverse velocity also contributes to effective temperatures. However, since the

collective transverse velocity at the freeze-out does not strongly change in the considered energy range (see Fig. 2), effective temperatures closely follow the shape of the $\langle \varepsilon_{out} \rangle$ energy dependence. These inverse slopes T were deduced by fitting the calculated spectra by the formula

$$\frac{d^2N}{m_T \, dm_T \, dy} \propto (m_T)^{\lambda} \exp\left(-\frac{m_T}{T}\right), \tag{1}$$

where m_T and y are the transverse mass and rapidity, respectively, and λ is a parameter which is taken different in different experimental fits, see, e.g., [5, 23].

Numerical problems, discussed in Ref. [12], prevented us from simulations at RHIC energies. Already for the central Pb+Pb collision at the top SPS energy the code requires 7.5 GB of (RAM) memory. At the top RHIC energy, required memory is three order of magnitude higher, which is unavailable in modern computers.

III.   PROTONS

The 3FD model does not distinguish isotopic species. In particular, the proton and neutron are considered to be identical, i.e. the nucleon. Therefore, a spectrum of protons is just associated with the nucleon spectrum multiplied by the factor Z/A with Z and A being the charge and the mass number of colliding nuclei, respectively (in this paper we consider only identical colliding
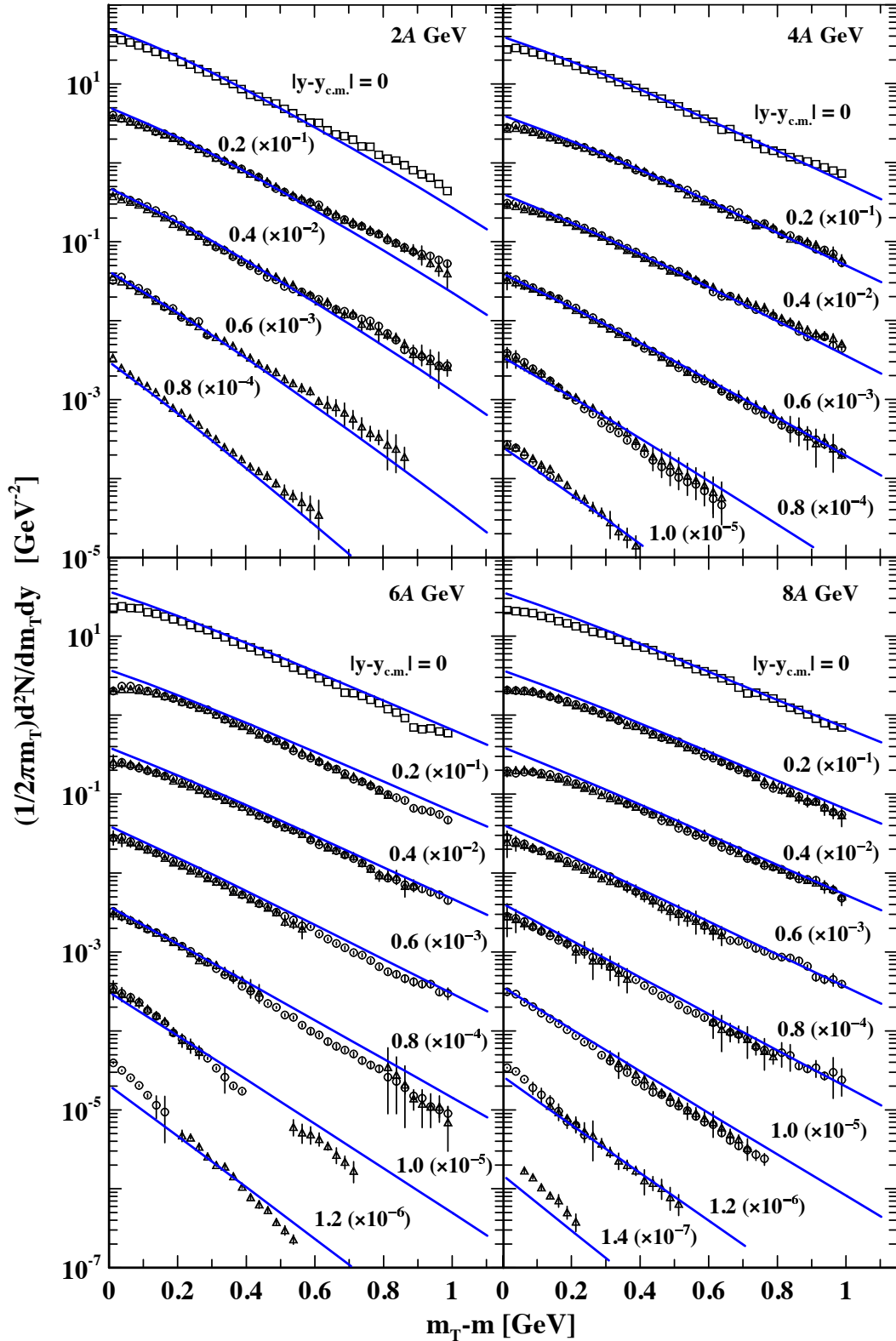
FIG. 4: (Color online) Transverse-mass spectra of protons in various rapidity bins (centered at $|y - y_{c.m.}|$) from central Au+Au collisions at incident energies $E_{\text{lab}} = 2A$, $4A$, $6A$, and $8A$ GeV. 3FD results are presented for impact parameter $b = 2$ fm. Midrapidity spectra are shown unscaled, while every next data set and the corresponding curve (from top to bottom) are multiplied by additional factor 0.1. Data are from E895 Collaboration [25]: open squares for midrapidity, circles for negative $(y - y_{c.m.})$ and triangles for positive $(y - y_{c.m.})$.
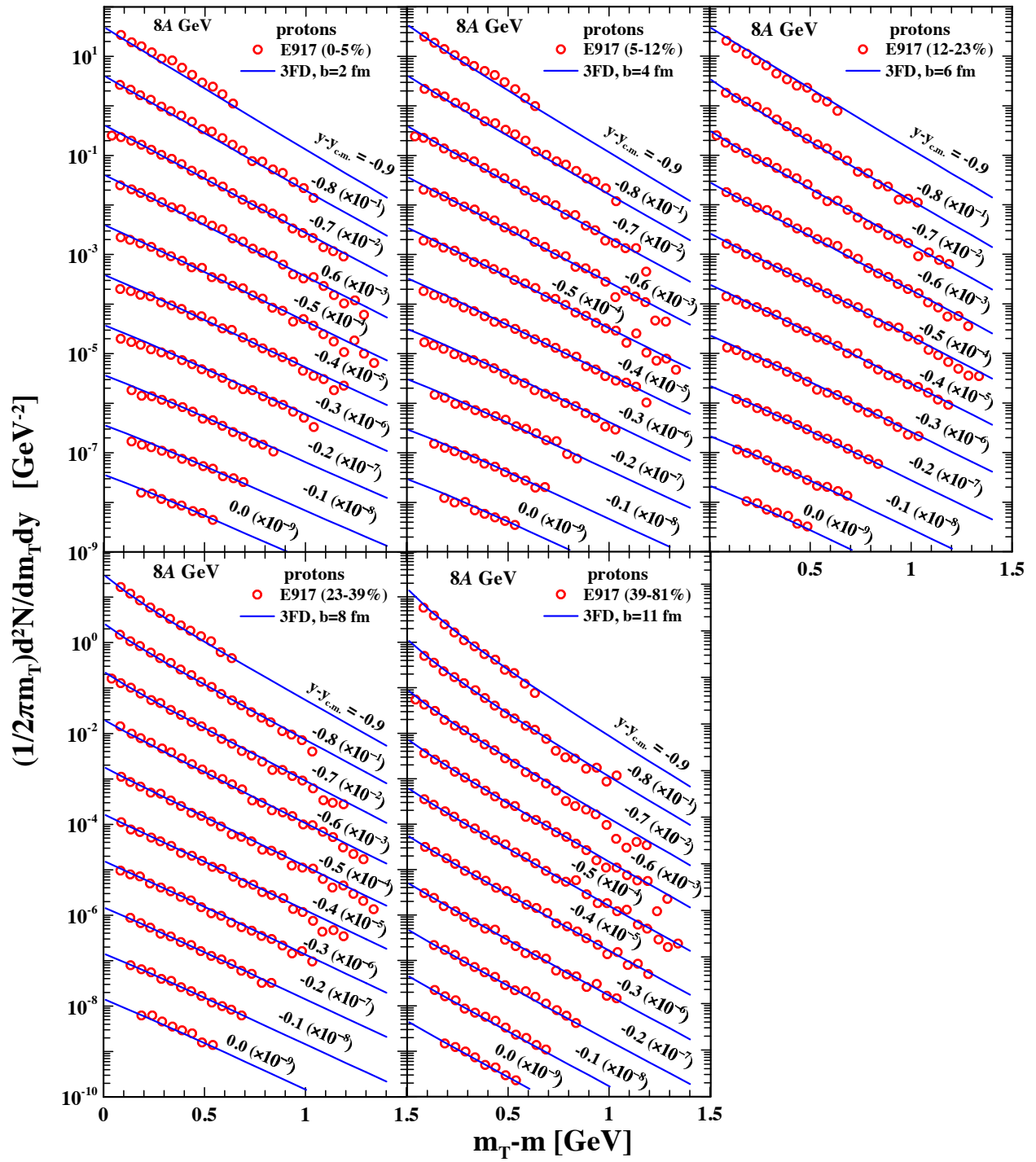
FIG. 5: (Color online) Transverse mass distributions of protons from Au(8A GeV)+Au collisions at various impact parameters (b) and in various rapidity bins (centered at $y - y_{c.m.}$). The most backward rapidity spectra are shown unscaled, while every next data set and the corresponding curve (from top to bottom) are multiplied by the additional factor 0.1. The percentage shows the fraction of the total reaction cross section, corresponding to experimental selection of events. Experimental data are from E917 Collaboration [26].

nuclei). This approximation is quite good at low incident energies, when the number of produced secondary particles (mostly pions) is well smaller than A. The particle production tends to restore isotopic symmetry. Hence,

the Z/A approximation becomes worse at high incident energies.

Reproduction of available transverse-mass spectra of protons is presented in Figs. 4–8. We consider here only
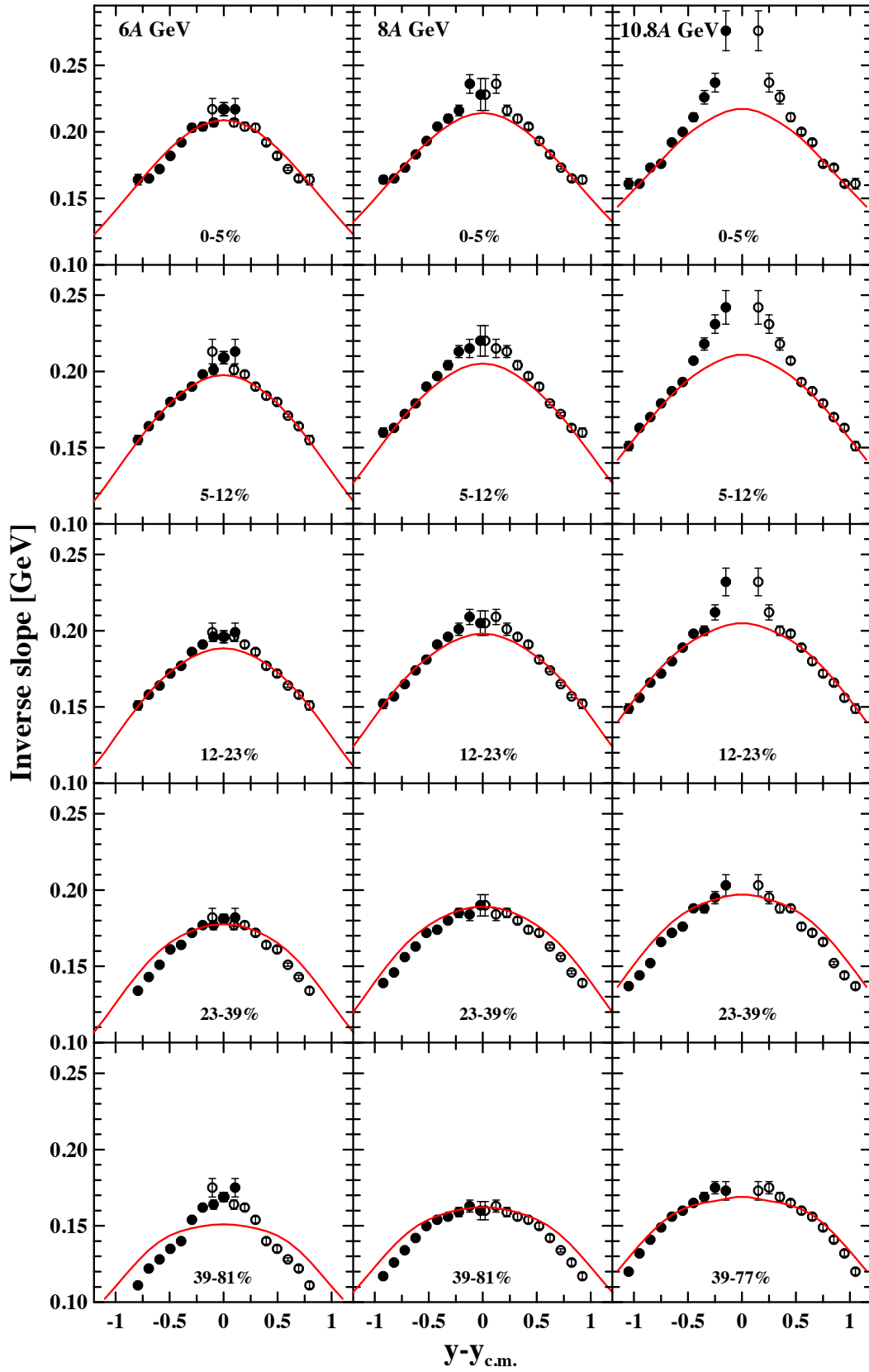
FIG. 6: (Color online) Inverse-slope parameters of transverse-mass spectra of protons produced in Au+Au collisions at incident energies $E_{\text{lab}} = 6A$, $8A$, $10.8A$ GeV at various centralities as a function of rapidity $y - y_{c.m.}$. 3FD results are presented for impact parameters $b = 2$, 4, 6, 8, and 11 fm (from top row of panels to bottom one). The percentage indicates the centrality, i.e. the fraction of the total reaction cross section, corresponding to experimental selection of events. Experimental data are from E917 Collaboration [23].
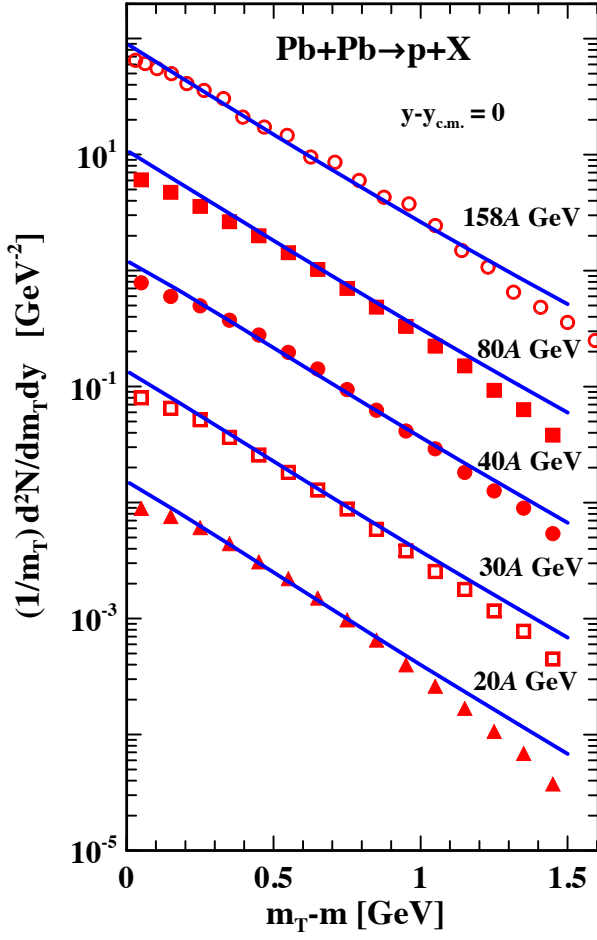
FIG. 7: (Color online) Transverse-mass distributions of protons at the midrapidity from central Pb+Pb collisions at incident energies $E_{\text{lab}} = 158A$, $80A$, $40A$ $30A$ and $20A$ GeV. 3FD results are presented for impact parameter $b = 2.5$ fm. The spectrum for $158A$ GeV energy is shown unscaled, while every next data set and the corresponding curve (from top to bottom) are multiplied by the additional factor 0.1. NA49 experimental data are taken from [27] ($158A$ GeV), [28] ($80A$ and $40A$ GeV) and [6] ($30A$ and $20A$ GeV).
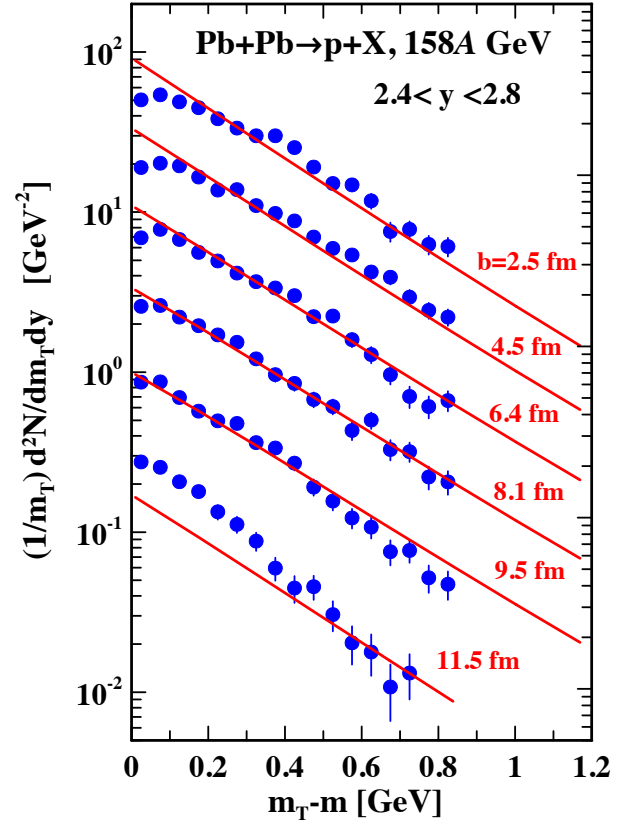

FIG. 8: (Color online) Transverse-mass distributions of protons in the rapidity range $2.4 < y < 2.8$ from Pb+Pb collisions at incident energy $E_{\text{lab}} = 158A$ GeV and various centralities, i.e., impact parameters b. The spectrum for central collisions is shown unscaled, while every next data set and the corresponding curve (from top to bottom) are multiplied by the additional factor 0.5. NA49 experimental data are taken from Ref. [24]. 3FD results are presented for rapidity $y = 2.6$ and impact parameters estimated in Ref. [24].

collisions of heavy nuclei, since they offer favorable conditions for application of the hydrodynamics. With few exceptions, overall reproduction of these spectra is quite good in terms of both normalization and slope.

The first exception is the spectrum at the lowest considered energy of $2A$ GeV, see Fig. 4. The calculated spectrum turns out to be steeper than the experimental one in all rapidity bins. This spectrum is calculated with our default choice of the freeze-out energy density $\varepsilon_{\text{frz}}(2A\text{ GeV}) = 0.3$ GeV/fm^3 accepted in our previous papers [10, 12, 14]. Variation of ε_{frz} in the range from 0.1 to 0.6 GeV/fm^3 does not noticeably affects the slope of the spectrum. This fact agrees with the above discussed dynamics of the freeze-out at low energies. Indeed, the surface freeze-out occurs at lower energy density which is the same independently of ε_{frz}. Only global freeze-

out of the system residue in the very end of the system disintegration produces slight sensitivity to ε_{frz}. This problem at the energy of $2A$ GeV indicates that the accepted model of the freeze-out is poorly applicable at low incident energies.

The 3FD model does not exhibit deviation from the exponential fall-off at $(m_T - m) \lesssim 0.2$ GeV, observed in the experiment, as it is most clearly seen in Figs. 4 and 8. The same feature of the hydrodynamic calculation was earlier reported in Ref. [29]. As it was shown [29], a post-hydro kinetic evolution (afterburner) is required to produce the observable two-slope structure of the m_T-spectra. In our model such a post-hydro evolution is absent. It is worthwhile to note that the above problem is not an inevitable feature of any hydrodynamic calculation. For instance, the deviation from the exponential fall-off was reproduced in calculations by Kolb *et al.* [30].

Traditionally, this deviation from the exponential fall-off at low $(m_T - m)$ is associated with collective trans-
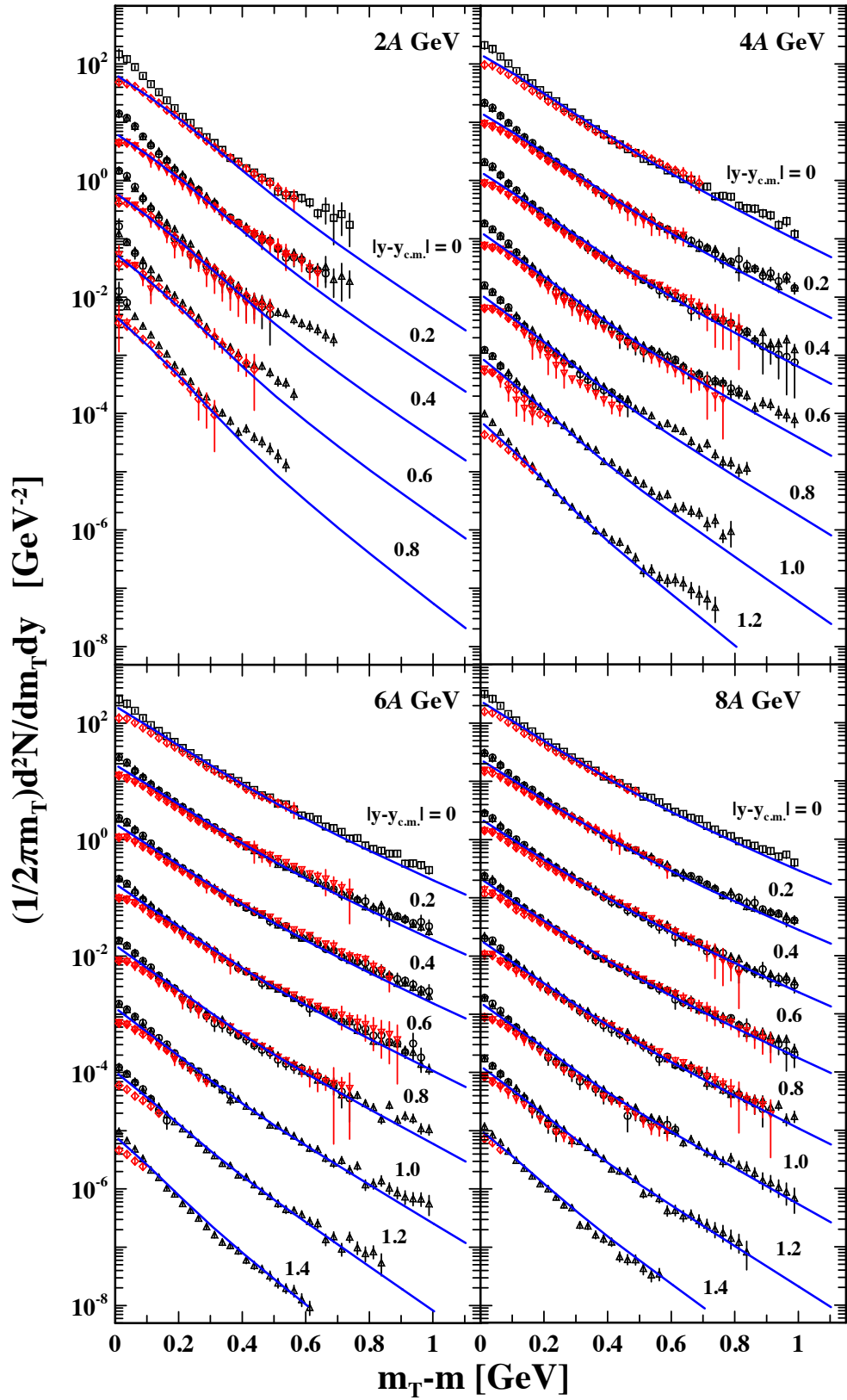
FIG. 9: (Color online) Transverse-mass spectra of positive and negative pions in various rapidity bins (centered at $|y - y_{c.m.}|$) for central Au+Au collisions at incident energies E_{lab} = 2A, 4A, 6A, and 8A GeV. 3FD results (for $(\pi^+ + \pi^0 + \pi^-)/3$) are presented for impact parameter $b = 2$ fm. Midrapidity spectra are shown unscaled, while every next data set and the corresponding curve (from top to bottom) are multiplied by the additional factor 0.1. Data are from the E895 Collaboration [32]: squares for midrapidity π^-, triangles for positive-rapidity π^-, circles for negative-rapidity π^-, diamonds for midrapidity and positive-rapidity π^+, inverted triangles for negative-rapidity π^+.
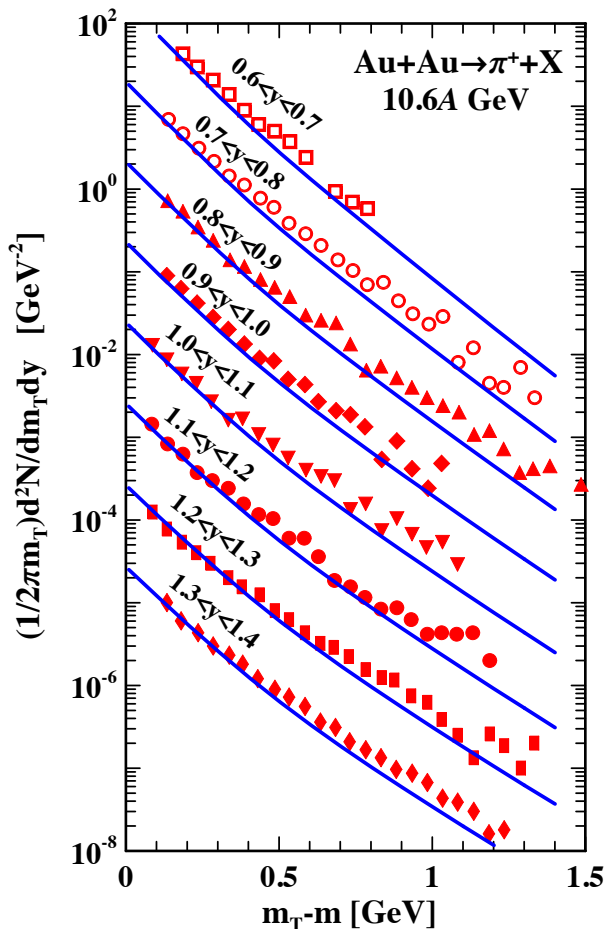
FIG. 10: (Color online) Transverse-mass spectra of positive pions in various rapidity bins from central Au+Au collisions at incident energy $E_{\mathrm{lab}} = 10.6A$ GeV. 3FD results (for $(\pi^+ + \pi^0 + \pi^-)/3$) are presented for impact parameter $b = 2$ fm. The most backward rapidity spectrum is shown unscaled, while every next data set and the corresponding curve (from top to bottom) are multiplied by the additional factor 0.1. Data are from the E802 Collaboration [33].

verse expansion of the system [29, 31]. In Ref. [29] it is described how the post-hydro cascade modify this radial flow. Apparently the final-stage (post-hydro) Coulomb interaction also distinctly affects the flow, accelerating or decelerating it depending on the electric charge of the species. It is clear from the difference between spectra of positive and negative pions, see Fig. 9. As seen from Fig. 9, negative pions are decelerated (their low-m_T spectrum is enhanced) while positive pions are accelerated (their low-m_T spectrum is suppressed). The same mechanism should also contribute to suppression of low-m_T spectrum of protons as compared to pure hydrodynamic calculation. With rapidity moving off the midrapidity, m_T-spectra of protons reveal weaker suppression of their low-m_T parts, see Fig. 4. This fact complies with the Coulomb mechanism. Indeed, faster particles (in the frame, where the fireball generating the field is at rest)

spend shorter time in the Coulomb field and, hence, acquire smaller additional momentum.

Thus, keeping in mind that reproduction of the data in the low-m_T region can be cured by application of a post-hydro dynamics, we see that, in general, the 3FD model reasonably reproduces proton m_T-spectra beyond extreme kinematic regions—rapidities being to far from the midrapidity and too high m_T (see Fig. 4)—in not too peripheral collisions of heavy nuclei (see Fig. 8). In the above marginal regions applicability of hydrodynamics is questionable. However, even in very peripheral collisions agreement with data can be unexpectedly good, see Fig. 5.

Inverse-slope parameters [cf. Eq. (1) with $\lambda = 1$], displayed in Fig. 6, summarize our results at AGS energies. The most pronounced disagreement with experimental temperatures occurs in midrapidity region, especially at $10.8A$ GeV incident energy. This problem is directly related to the above-discussed poor reproduction of low-m_T suppression of the spectra. Apart from this problem, effective temperatures are well reproduced.

IV. PIONS

Comparison of calculated transverse-mass spectra of pions with available data is presented in Figs. 9–12. Since the 3FD model does not distinguish isotopic species, we assume that numbers (and spectra) of π^+, π^- and π^0 are identical and equal $1/3$ of the total number (spectrum) of pions. In view of this approximation, if calculated spectra are situated between measured spectra of positive and negative pions, that would mean a good agreement of our calculations with data. Contrary to protons, this approximation becomes better applicable at high incident energies, when abundant production of secondary particles results in partial restoration of isotopic symmetry of the system. As it is illustrated in Fig. 9, spectra of positive and negative pions indeed become more and more similar with the incident energy rise.

Similarly to the proton case, agreement with data is the worst at the lowest considered incident energy of $2A$ GeV, see Fig. 9. There our calculated spectra closely follow experimental spectra for positive pions, while they should lie in between π^+ and π^- spectra. Above this energy, overall reproduction of pion spectra is quite good both in normalization and slope. It is even better than that for protons. The calculated pion spectra also reproduce the rapidity (Figs. 9 and 10) and incident-energy (Figs. 11 and 12) dependence of the data. Note that this agreement is achieved with the unified chemical-thermal freeze-out. Of course, two different freeze-out criteria for chemical and thermal processes could slightly improve this agreement with the experiment. However, that would be too high price for so tiny improvement.
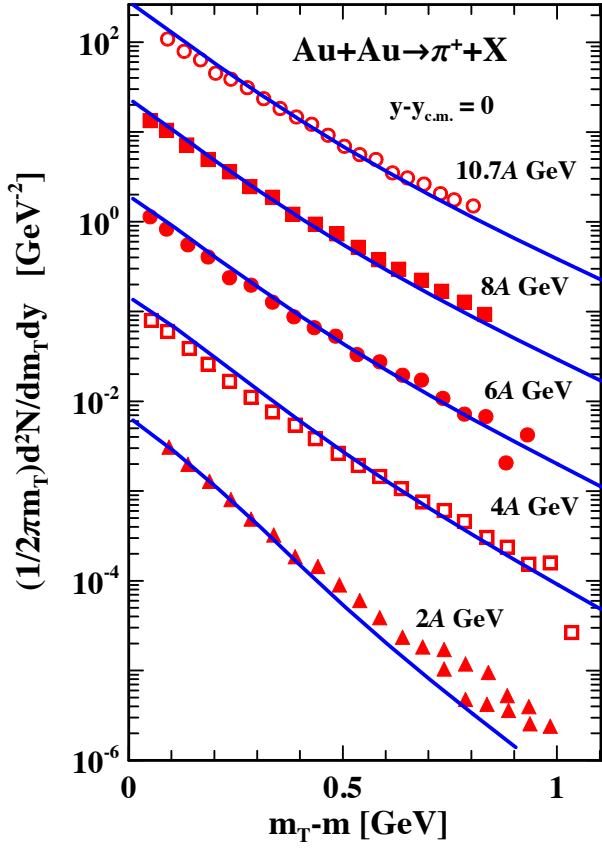
FIG. 11: (Color online) Transverse-mass spectra of positive pions at midrapidity in central Au+Au collisions at incident energies $E_{lab} = 2A$, $4A$, $6A$, $8A$, and $10.7A$ GeV. 3FD results (for $(\pi^+ + \pi^0 + \pi^-)/3$) are presented for impact parameter $b = 2$ fm. Spectrum for $10.7A$ GeV is shown unscaled, while every next data set and the corresponding curve (from top to bottom) are multiplied by the additional factor 0.1. Data are from the E866 Collaboration [5].

FIG. 12: (Color online) Transverse-mass spectra of negative pions at midrapidity in central Pb+Pb collisions at various incident energies $E_{lab} = 20A$, $30A$, $40A$, $80A$, and $158A$ GeV. 3FD results (for $(\pi^+ + \pi^0 + \pi^-)/3$) are presented for impact parameter $b = 2.5$ fm. The spectrum for $158A$ GeV energy is shown unscaled, while every next data set and the corresponding curve (from top to bottom) are multiplied by the additional factor 0.1. Data are from the NA49 Collaboration [7].

V.   KAONS

Upon demonstrating that calculated proton and pion transverse-mass spectra are in reasonable agreement with available data we proceed to kaon spectra. The "step-like" incident energy dependence of the the inverse-slope parameter (T, cf. Eq. (1)) of these spectra was interpreted as a signal of the deconfinement phase transition [8, 9]. Moreover, microscopic transport models, based on hadronic degrees of freedom, failed to reproduce the observed behavior of the kaon inverse slope [2, 3].

Comparison of calculated of transverse-mass spectra of kaons with available data in collisions of heavy nuclei is presented in Figs. 13–16. Overestimation of kaon normalization at low incident energies ($E_{lab} \lesssim 6A$ GeV) is not surprising, see Fig. 14. This is not a result of the unified chemical-thermal freeze-out. The reason is that we use the EoS based on grand canonical ensemble, therefore production of rare particles should be overestimated at low energies. This normalization can be easily corrected
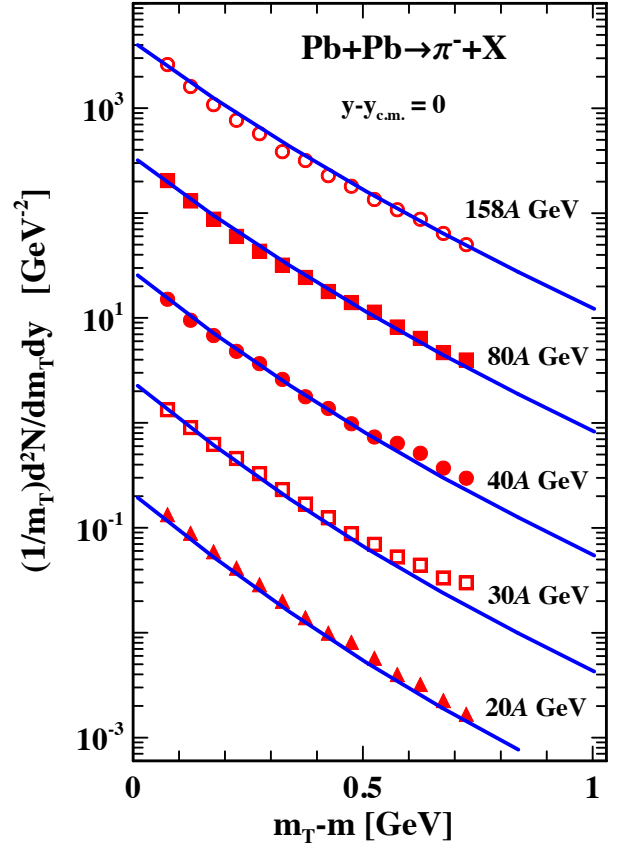
by introducing a suppression factor γ_s, taking into account associative production of strangeness. Apart from this normalization, overall reproduction of kaon spectra is quite satisfactorily. Separate treatment of the chemical and thermal freeze-outs could certainly improve the normalization of kaon spectra at SPS energies. However, to do this we would have to introduce different freeze-out criteria for K^+ and K^-. This is distinctly seen, e.g., at the example of K^+ and K^- spectra at $E_{lab} = 80A$ GeV, see Figs. 15 and 16. The K^+ spectrum requires somewhat earlier freeze-out in order to increase the normalization. While the K^- spectrum demands for later freeze-out to reduce the normalization. In fact, there are physical arguments in favor of this sequence of K^+ and K^- freeze-outs. We prefer a cruder description of observables to introduction of additional fitting parameters.

Dependence on the rapidity is reproduced, see Fig. 13, as well as evolution of slopes with the incident energy variation, see Figs. 13–16. Fig. 3 demonstrates that
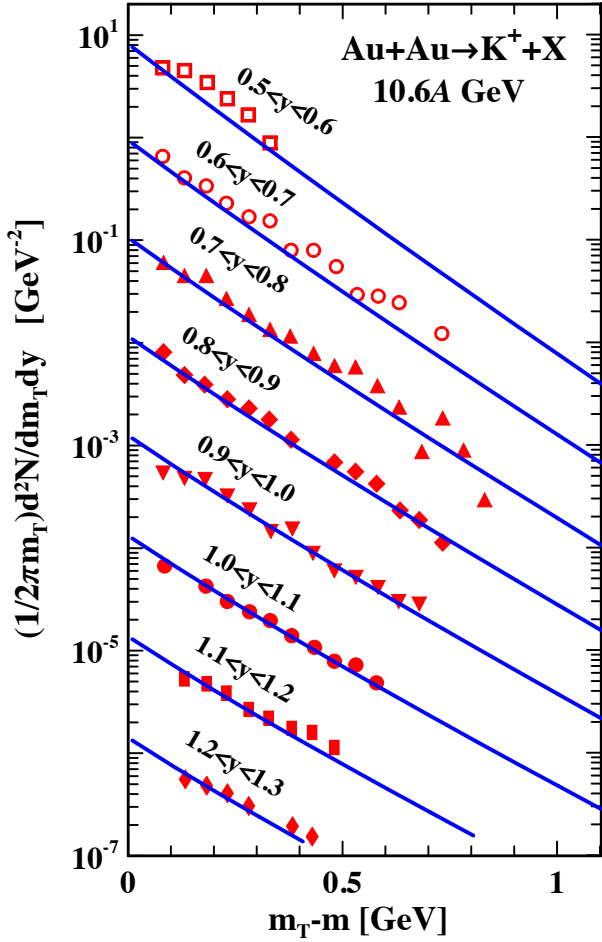
FIG. 13: (Color online) Transverse-mass spectra of positive kaons in various rapidity bins in central Au+Au collisions at incident energy $E_{\text{lab}} = 10.6A$ GeV. 3FD results are presented for impact parameter $b = 2$ fm. The most backward rapidity spectrum is shown unscaled, while every next data set and the corresponding curve (from top to bottom) are multiplied by the additional factor 0.1. Data are from the E802 Collaboration [33].
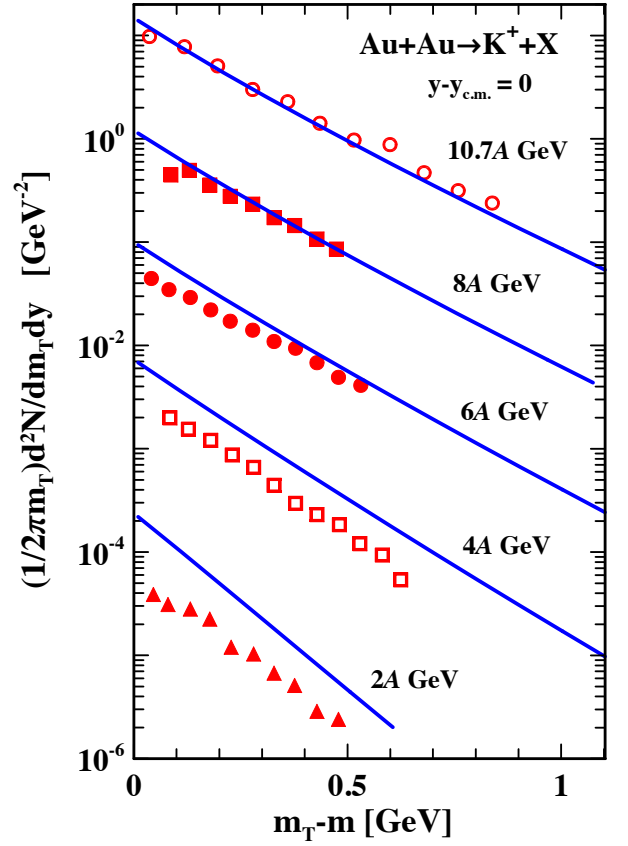

FIG. 14: (Color online) Transverse-mass spectra of positive kaons at midrapidity in central Au+Au collisions at incident energies $E_{\text{lab}} = 2A$, $4A$, $6A$, $8A$, and $10.7A$ GeV. 3FD results are presented for impact parameter $b = 2$ fm. Spectrum for $10.7A$ GeV is presented unscaled, while every next data set and the corresponding curve (from top to bottom) are multiplied by the additional factor 0.1. Data are from the E866 Collaboration [5].

inverse slopes of kaon spectra are indeed reasonably reproduced. This inverse slopes were deduced by fitting the calculated spectra by formula (1) with $\lambda = 0$ (purely exponential fit). Moreover, the pion and proton effective temperatures also reveal saturation at SPS energies, if they are deduced from the same purely exponential fit with $\lambda = 0$. Though the purely exponential fit with $\lambda = 0$ does not always provide the best fit of the spectra, it allows a systematic way of comparing spectra at different incident energies. In order to comply with experimental fits at AGS energies (and hence with displayed experimental points displayed by squares), we also present results of fits with $\lambda = -1$ for pions and with $\lambda = 1$ for protons. The most pronounced disagreement with experimental temperatures takes place for protons, while reproduction of the proton spectra themselves (see Fig. 7) does not look bad.

VI.   SUMMARY

Transverse-mass spectra of protons, pions and kaons in wide ranges of incident energies (from AGS to SPS), rapidity bins and centralities have been analyzed within the 3FD model. These spectra were computed with the same set of model parameters as that summarized in Ref. [12]. In particular, the hadronic EoS [16] with incompressibility $K = 210$ MeV was used. We considered here only collisions of heavy nuclei, since they offer favorable conditions for application of the hydrodynamics. It was demonstrated that with few exceptions the 3FD model reasonably reproduces these spectra in the range of incident energies $4A$ GeV $\lesssim E_{\text{lab}} \lesssim 160A$ GeV. The exceptions concern extreme kinematic regions—rapidities being to far from midrapidity and too high m_T—and too peripheral collisions of heavy nuclei. In the above marginal regions applicability of the hydrodynamics is questionable. However, even in very peripheral collisions agreement with data can be unexpectedly good.
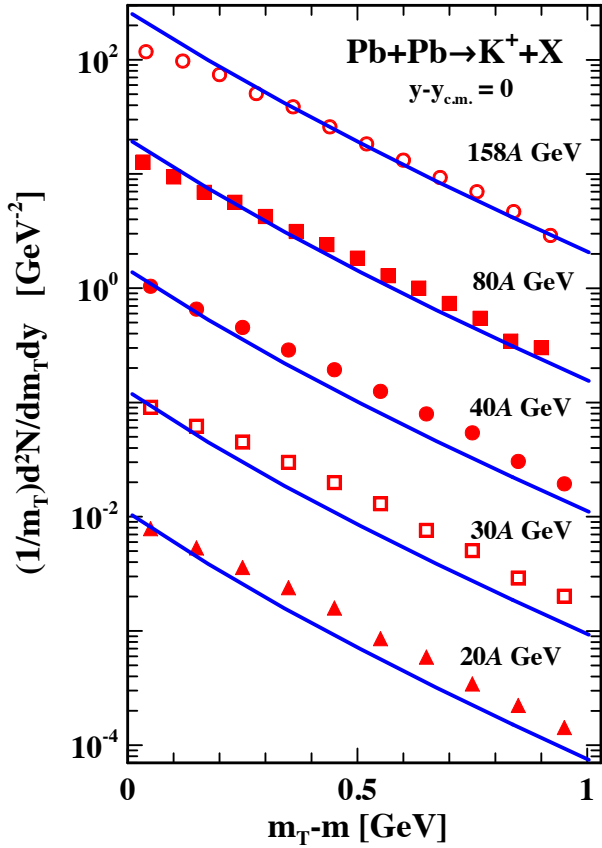
FIG. 15: (Color online) Transverse-mass spectra of positive kaons at midrapidity in central Pb+Pb collisions at various incident energies $E_{\text{lab}} = 20A$, $30A$, $40A$, $80A$, and $158A$ GeV. 3FD results are presented for impact parameter $b = 2.5$ fm. The spectrum for $158A$ GeV energy is shown unscaled, while every next data set and the corresponding curve (from top to bottom) are multiplied by the additional factor 0.1. Data are from the NA49 Collaboration [7].

FIG. 16: (Color online) The same as in Fig. 15 but for negative kaons.

The 3FD model reproduces inverse slopes of m_T-spectra, in particular, the "step-like" dependence of kaon inverse slopes on the incident energy. This hydrodynamic explanation of the transverse-mass spectra and "step-like" behavior of effective temperatures implies that at considered incident energies a heavy nuclear system really reveals a hydrodynamic motion during its expansion.

In fact, microscopic transport and hydrodynamic models do not contradict each other. The fact that they all successfully describe many observales in collisions heavy nuclei in spite of big differences between these models suggests that detailed information on cross sections is unimportant for these reactions. The collision frequency is already high enough in order to make hydrodynamics to be applicable. This conjecture has already been put forward in Ref. [34]. In particular, transport [2, 3] and hydrodynamic models well describe pion transverse-mass spectra of pions in wide range of incident energies. Therefore, the failure of microscopic transport models [2, 3] to reproduce the observed behavior of the kaon
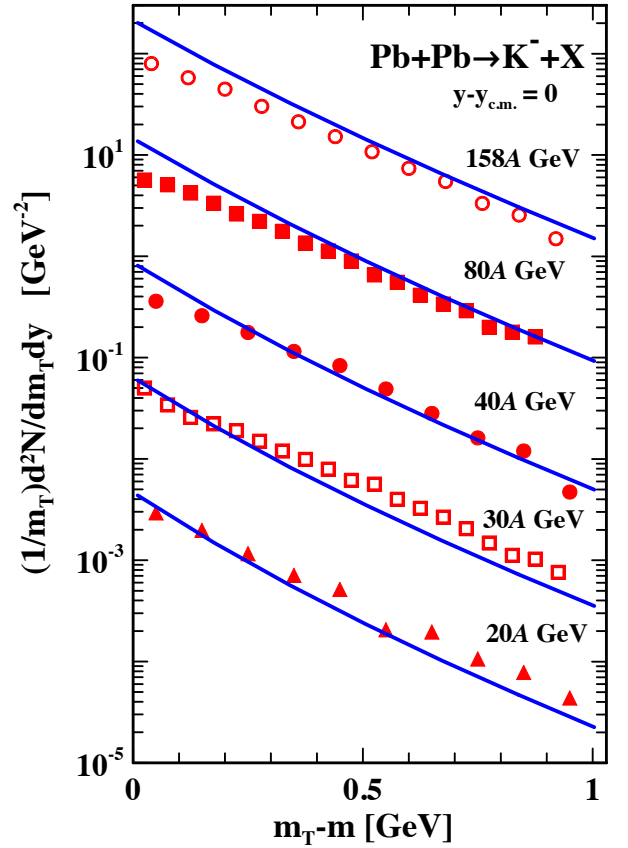
inverse slopes may be interpreted as a signature that kaon and antikaon interaction cross sections in microscopic models are not big enough for kaons to be captured by matter in a common flow. In Ref. [2] a kind of such cross-section enhancement (Cronin effect) was tested against the experimental data. The resulting effect of that enhancement was found insufficient to explain the observed discrepancy. Another possibility is that multi-body collisions are important in the transport. This was checked within the Giessen Boltzmann-Uehling-Uhlenbeck (GiBUU) model [35], where three-body interactions were included in simulations. It was found that the three-body collisions indeed result in good reproduction of all transverse-mass spectra [35].

Returning to the question if the considered "step-like" behavior of effective temperatures is a signal of a phase transition into the QGP, we have to admit that this is not quite clear as yet. It depends on the nature of the freeze-out parameter $\varepsilon_{\text{frz}} = 0.4$ GeV/fm^3 which should be further clarified. The EoS is not of prime importance for this behavior. The only constraint on the EoS is that it should be in some way reasonable. Moreover, our preliminary results indicate that a completely different (from that used in this work) EoS [36] with 1st order phase transition to the QGP still reasonably reproduces this "step-like" behavior even in spite of that it fails to de-

scribe a large body of other data. This happens because the same freeze-out pattern is accepted there.

This kind of the freeze-out has its implications for observation of fluctuations. A number of observables were suggested, which are based on various fluctuations: transverse-momentum fluctuations [37], electric-charge fluctuations [38, 39], baryon-charge–strangeness correlations [40], fluctuations of the K/π ratio [41]; for the recent review see Ref. [42]. These observables distinguish between the hadronic and quark–gluon phases. However, available experimental data on fluctuations: on p_T fluctuations [43, 44, 45, 46] and positive-to-negative charge-ratio fluctuations [47, 48], at SPS energies well agree with the hadronic predictions. Only the K/π fluctuations [49] reveal a nontrivial behaviour with the incident energy.

The fact that the freeze-out takes place at rather low values of energy density and temperature (see Figs. 1 and 2) explains why we observe only hadronic fluctuations at the freeze-out, even if the compressed matter was in the quark–gluon phase. All the quark–gluon fluctuations get dissolved during the long path of the system from hadronization to freeze-out. Fluctuations of the K/π ratio can be an exception from this rule, since this signal is the most robust. A K^+ meson can disappear only if it meets a particle of the opposite strangeness (Λ, Σ or K^-). If the strange system is relatively dilute at the hadronic stage of the expansion, as it is the case at lower SPS energies, the probability to meet a particle of the opposite strangeness is relatively low. Therefore, the signal from the quark–gluon phase par-

tially survives. At higher energies (top SPS energies) the strange system becomes already dense enough to destroy this signal. This mechanism can explain a non-trivial energy dependence of the K/π fluctuations, observed by the NA49 Collaboration [49]. It implies violation of the chemical equilibrium for strange particles at the late stage of the expansion. Therefore, it is beyond the frame of the present version of the 3FD model, where K^+ meson abundance immediately follow changes of densities of the matter. If this explanation is true, fluctuations of the ratio $K^+/\pi^+ = N_{K^+}/N_{\pi^+}$ should reveal even stronger energy dependence than those of the ratio $K/\pi = (N_{K^+} + N_{K^-})/(N_{\pi^+} + N_{\pi^-})$, where N_a is the observed yield of a-particles. The same mechanism can be behind the horn effect in the excitation function of the K^+/π^+ ratio [50].

Acknowledgements

[1] R. Stock, J. Phys. G **30**, 633 (2004).
[2] E.L. Bratkovskaya, S. Soff, H. Stoecker, M. van Leeuwen, and W. Cassing, Phys. Rev. Lett. **92**, 032302 (2004); E.L. Bratkovskaya, M. Bleicher, M. Reiter, S. Soff, H. Stoecker, M. van Leeuwen, S. Bass, and W. Cassing, Phys. Rev. C **69**, 054907 (2004).
[3] M. Wagner, A.B. Larionov, and U. Mosel, Phys. Rev. C **71**, 034910 (2005).
[4] M. Gazdzicki, M.I. Gorenstein, F. Grassi, Y. Hama, T. Kodama, and O. Socolowski Jr, Braz. J. Phys. **34**, 322 (2004).
[5] L. Ahle, *et al.* (E866 and E917 Collaborations), Phys. Lett. **B476**, 1 (2000).
[6] M. Gazdzicki, *et al.* (NA49 Collab.), J. Phys. **G30**, S701 (2004).
[7] S. V. Afanasiev, *et al.* (NA49 Collab.), Phys. Rev. C **66**,054902 (2002); C. Alt, *et al.* (NA49 Collab.), J. Phys. **G30**, S119 (2004).
[8] M.I. Gorenstein, M. Gazdzicki, and K. Bugaev, Phys. Lett. **B567**, 175 (2003).
[9] B. Mohanty, J. Alam, S. Sarkar, T.K. Nayak, B.K. Nandi, Phys. Rev. C **68**, 021901 (2003).
[10] Yu.B. Ivanov and V.N. Russkikh, Eur. Phys. J. **A 37**, 139 (2008).
[11] V.N. Russkikh and Yu.B. Ivanov, Phys. Rev. C **76**, 054907 (2007).
[12] Yu.B. Ivanov, V.N. Russkikh, and V.D. Toneev, Phys.

Rev. C **73**, 044904 (2006).
[13] V.D. Toneev, Yu.B. Ivanov, E.G. Nikonov, W. Norenberg, and V.N. Russkikh, Phys. Part. Nucl. Lett. **2**, 288 (2005); V.N. Russkikh, Yu.B. Ivanov, E.G. Nikonov, W. Norenberg, and V.D. Toneev, Phys. Atom. Nucl. **67**, 199 (2004).
[14] V.N. Russkikh and Yu.B. Ivanov, Phys. Rev. C **74**, 034904 (2006).
[15] Yu.B. Ivanov and V.N. Russkikh, PoS(CPOD07)008 (2007), arXiv:0710.3708 [nucl-th].
[16] V.M. Galitsky and I.N. Mishustin, Sov. J. Nucl. Phys. **29**, 181 (1979).
[17] F. Grassi, Y. Hama, and T. Kodama, Phys. Lett. **B355**, 9 (1995); Z. Phys. **C73**, 153 (1996); Yu.M. Sinyukov, S.V. Akkelin, and Y. Hama, Phys. Rev. Lett. **89**, 052301 (2002); F. Grassi, Braz. J. Phys. **35**, 52 (2005).
[18] S.V. Akkelin, Y. Hama, Iu.A. Karpenko, and Yu.M. Sinyukov, arXiv:0804.4104v3 [nucl-th].
[19] J. Knoll, arXiv:0803.2343 [nucl-th]
[20] A. Andronic, P. Braun-Munzinger, and J. Stachel, Nucl. Phys. **A772**, 167 (2006);
[21] J. Cleymans, H. Oeschler, and K. Redlich, hep-ph/0607164; J. Cleymans, H. Oeschler, K. Redlich, and S. Wheaton, Phys. Rev. C **73**, 034905 (2006)
[22] J. Randrup and J. Cleymans, Phys. Rev. **C 74**, 047901 (2006)
[23] B.B. Back *et al.* (E917 Collab.), Phys. Rev. C **66**, 054901

(2002).

[24] T. Anticic *et al.* (NA49 Collab.), Phys. Rev. C **69**, 024902 (2004). C. Alt *et al.* (NA49 Collab.), Phys. Rev. C **73**, 044910 (2006).

[25] J.L.Klay, *et al.* (E895 Collab.), Phys. Rev. Lett. **88**, 102301 (2002)

[26] B.B. Back *et al.* (E917 Collab.), Phys. Rev. Lett. **86** , 1970 (2001).

[27] H. Appelshäuser *et al.* (NA49 Collab.), Phys. Rev. Lett. **82**, 2471 (1999).

[28] M. van Leeuwenet *et al.* (NA49 Collab.), Nucl. Phys. **A715**, 161c (1999).

[29] D. Teaney, J. Lauret, and E.V. Shuryak, nucl-th/0110037, Phys. Rev. Lett. **86**, 4783, (2001).

[30] P. Huovinen, P.V. Ruuskanen and J. Sollfrank, Nucl. Phys. **A650**, 227 (1999); P.F. Kolb, J. Sollfrank, P.V. Ruuskanen, and U. Heinz, Nucl. Phys. **A661**, 349 (1999); P.F. Kolb and U. Heinz, in "Quark Gluon Plasma 3", p. 634, Eds. R.C. Hwa and X.N. Wang, World Scientific 2003, Singapore; P. Huovinen and P.V. Ruuskanen, Submitted to Ann.Rev.Nucl.Part.Sci., nucl-th/0605008.

[31] P.J. Siemens and J.O. Rasmussen, Phys. Rev. Lett. **42**, 880 (1979); E.V. Shuryak and O.V. Zhirov, Phys. Lett. **B89**, 253 (1979); E. Schnederman, J. Sollfrank, U.Heinz, Phys. Rev. C**48**, 2462 (1993).

[32] J.L. Klay, *et al.* (E895 Collab.), Phys. Rev. C **68**, 054905 (2003)

[33] L. Ahle, *et al.* (E802 Collab.), Phys. Rev. C **59**, 2173 (1999).

[34] C.M. Hung and E.V. Shuryak, Phys. Rev. Lett. **75**, 4003 (1995); C.M. Hung and E. Shuryak, Phys. Rev. C **57**, 1891 (1998).

[35] A.B. Larionov, O. Buss, K. Gallmeister, and U. Mosel, Phys.Rev. C **76**, 044909 (2007).

[36] A.S.Khvorostukhin, V.V. Skokov, K. Redlich, and V.D. Toneev, Eur. Phys. J. **C48**, 531 (2006).

[37] M.A. Stephanov, K. Rajagopal, and E.V. Shuryak, Phys. Rev. Lett. **81**, 4816 (1998); Phys. Rev. D **60**, 114028 (1999).

[38] S. Jeon and V. Koch, Phys. Rev. Lett. **85**, 2076 (2000).

[39] M. Asakawa, U. W. Heinz, and B. Muller, Phys. Rev. Lett. **85**, 2072 (2000).

[40] V. Koch, A. Majumder, and J. Randrup, Phys. Rev. Lett. **95**, 182301 (2005).

[41] V. Koch, A. Majumder, and J. Randrup, Phys. Rev. C **72**, 064903 (2005).

[42] V. Koch, arXiv:0810.2520 [nucl-th].

[43] H. Sako and H. Appelshaeuser (CERES/NA45 Collab.), J. Phys. **G30**, S1371 (2004).

[44] H. Appelshauser, *et al.* (NA49 Collab.), Phys. Lett. **B459**, 679 (1999).

[45] M. Rybczynski, *et al.* (NA49 Collab.), arXiv:0805.2245 [nucl-ex].

[46] K. Grebieszkow, *et al.* (NA49 Collab.), PoS(CPOD07)022 (2007), arXiv:0707.4608 [nucl-ex].

[47] C. Alt, *et al.* (NA49 Collab.), Phys. Rev. C **70**, 064903 (2004).

[48] H. Appelshauser, *et al.* (CERES Collab.), Nucl. Phys. **A752**, 394 (2005).

[49] C. Alt, *et al.* (NA49 Collab.), arXiv:0808.1237 [nucl-ex].

[50] C. Alt, *et al.* (NA49 Collab.), Phys. Rev. C **77**, 024903 (2008).